

# Subsurface Flows in and Around Active Regions with Rotating and Non-rotating Sunspots

K. Jain · R.W. Komm ·  
I. González Hernández · S.C. Tripathy ·  
F. Hill

© Springer ....

**Abstract** The temporal variation of the horizontal velocity in subsurface layers beneath three different types of active regions is studied using the technique of ring diagrams. In this study, we select active regions (ARs) 10923, 10930, 10935 from three consecutive Carrington rotations: AR 10930 contains a fast-rotating sunspot in a strong emerging active region while other two have non-rotating sunspots with emerging flux in AR 10923 and decaying flux in AR 10935. The depth range covered is from the surface to about 12 Mm. In order to minimize the influence of systematic effects, the selection of active and quiet regions is made so that these were observed at the same heliographic locations on the solar disk. We find a significant variation in both components of the horizontal velocity in active regions as compared to quiet regions. The magnitude is higher in emerging-flux regions than in the decaying-flux region, in agreement with earlier findings. Further, we clearly see a significant temporal variation in depth profiles of both zonal and meridional flow components in AR 10930, with the variation in the zonal component being more pronounced. We also notice a significant influence of the plasma motion in areas closest to the rotating sunspot in AR 10930 while areas surrounding the non-rotating sunspots in all three cases are least affected by the presence of the active region in their neighborhood.

**Keywords:** Helioseismology, Observations - Interior, Convection Zone - Velocity Fields, Interior - Sunspots, Velocity

## 1. Introduction

Many intriguing studies related to the Sun in recent years have been focused on deriving detailed information about active regions (ARs). Basically, these are the regions with high magnetic field concentration that may consist of one sunspot or an ensemble of several sunspots. The sunspots are seen to move across the disk

---

<sup>1</sup> National Solar Observatory, Tucson, AZ 85719, USA  
email: kjain@nso.edu email: rkomm@nso.edu email:  
irenegh@nso.edu email: stripathy@nso.edu email: fhill@nso.edu

for a long time and have been used to estimate differential rotation in the convection zone (*e.g.* Javaraiah, Bertello, and Ulrich, 2005; Hathaway and Wilson, 1990; and references therein). However, in some cases, these sunspots are also seen to rotate around their umbral centers or other sunspots within the same active region. The sunspots in this category are generally known as “rotating sunspots” (Evershed, 1909; Knoska, 1975; Brown *et al.*, 2003; Min and Chae, 2009). Studies suggest that there is no preferential direction for their rotation, some rotate in clockwise direction while others in anti-clockwise direction. Furthermore, this kind of rotation may lead to the buildup of energy, which might be later released by a flare (Stenflo, 1969). The origin of such rotational motion is thought to arise from the shear and twist in magnetic-field lines or *vice versa*. It is also suggested that the magnetic twist may result from the disturbance in large-scale flows in the solar convection zone and the photosphere or sub-photospheric layers (López Fuentes *et al.*, 2003).

In order to explore the dynamics beneath the solar surface, one may use the techniques of local helioseismology, which are capable of probing the solar interior in three dimensions (Antia and Basu, 2007; Gizon, Birch, and Spruit, 2010; and references therein). These techniques allow us to infer flows in different layers from the surface to several Mm in depth. For example, Zhao and Kosovichev (2003) applied the method of time–distance analysis to Michelson Doppler Imager (MDI) Dopplergrams to infer sub-photospheric vertical flows in a fast rotating sunspot region (AR 9114) and found evidence for two opposite vertical flows in the depth range of 0–12 Mm. Strong converging flows were found in the upper layers (0–3 Mm) while divergent flows were observed in deeper layers (9–12 Mm). Another technique, the ring-diagram method, has also been used to study flows in sub-surface layers in synoptic maps and active regions (Haber *et al.*, 2002; González Hernández *et al.*, 2006; Komm *et al.*, 2004, 2009). To verify the reliability of the results obtained with different techniques, Hindman *et al.* (2004) carried out a detailed comparison of horizontal flows using data from two years of the MDI Dynamics Program and found a good correlation between flows obtained with ring-diagram and time–distance methods.

In this article, we apply the ring-diagram technique to investigate the horizontal velocity in sub-photospheric layers beneath three active regions. Previous studies using this technique for active regions are mostly limited to average behavior summed over many regions irrespective of their dynamical characteristics (*e.g.* Komm, Howe, and Hill, 2011; and references therein). Thus, the temporal behavior of sub-surface flows in individual active regions is not fully addressed. Here, we categorize active regions on the basis of their characteristics and examine sub-surface horizontal velocity in and around those regions. We further investigate how velocity components beneath a rotating sunspot differ from that in a non-rotating sunspot. We infer depth profiles in the outer 2% of the solar interior by inverting velocities obtained from ring diagrams, which is briefly described in Section 2. The selection of data is discussed in Section 3. Finally, results are presented in Section 4 and summarized in Section 5.

## 2. Technique

In the ring-diagram technique, medium to high-degree acoustic modes are used to infer the characteristics of the propagating waves in localized areas of the solar surface (Hill, 1988). This method has been extensively used to study subsurface properties of both active and quiet regions (Rajaguru, Basu, and Antia, 2001; Basu, Antia, and Bogart, 2004; Jain *et al.*, 2008; Bogart *et al.*, 2008; Tripathy *et al.*, 2008; Komm *et al.*, 2008, 2009; Komm, Howe, and Hill, 2011, Baldner, Bogart, and Basu, 2011). In this analysis, we select an area of  $\approx 11^\circ \times 11^\circ$  centered on the active region on each image and tracked for 1680 minutes (referred to as one ring day in this article) using the surface rotation rate (Snodgrass, 1984). Each tracked area is apodized with a circular function and then a three-dimensional FFT is applied on both spatial and temporal direction to obtain a three-dimensional power spectrum. We fit the corresponding power spectrum using a Lorentzian profile model (Haber *et al.*, 2000),

$$P(k_x, k_y, \omega) = \frac{A}{(\omega - \omega_0 + k_x U_x + k_y U_y)^2 + \Gamma^2 + \frac{b}{k^3}} \quad (1)$$

where  $P$  is the oscillation power for a wave with a temporal frequency ( $\omega$ ) and the total wave number  $k^2 = k_x^2 + k_y^2$ . There are six parameters to be fitted: two Doppler shifts ( $k_x U_x$  and  $k_y U_y$ ) for waves propagating in the orthogonal zonal and meridional directions, the background power ( $b$ ), the mode central frequency ( $\omega_0$ ), the mode width ( $\Gamma$ ), and the amplitude ( $A$ ). Finally, the fitted velocities ( $U_x$  and  $U_y$ ) are inverted using regularized least square (RLS) method to estimate depth dependence of various components of the horizontal velocity.

## 3. Selection of Data

In this study, we focus on three isolated active regions: ARs 10923, 10930 and 10935. Sample continuum images of these regions for three consecutive days are shown in Figure 1. All three regions were observed around the same latitude band in the southern hemisphere in three successive Carrington rotations during the declining phase of solar cycle 23 and located in areas relatively free from other magnetic activity. In addition, our analysis is confined to those days when all three regions were also positioned at the same heliographic locations. This selection minimizes the influence of systematic errors on inferences that may arise due to the location of regions analyzed. Since new region numbers are assigned whenever regions appear on the east limb irrespective of their reappearance after completing a solar rotation, AR 10930 appears to be the same as 10923 in the preceding rotation and AR 10935 in the following rotation. However, all these regions exhibited different characteristics during their front-side disk passages and are considered independent active regions. It can be seen in Figure 1 that AR 10930 had two major sunspots; the big sunspot did not show any visible

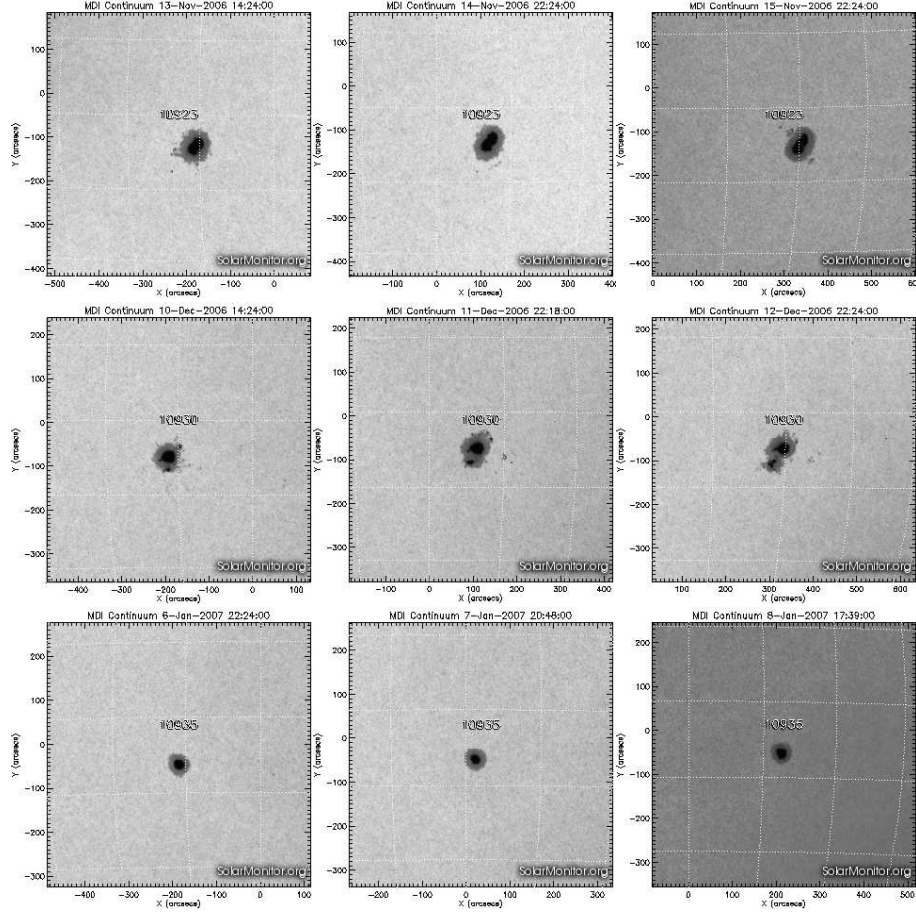


**Figure 1.** Examples of MDI continuum images of active regions used in this study for three consecutive days. Top: AR 10923 with non-rotating sunspots; Middle: AR 10930 with a group of non-rotating and rotating sunspots; Bottom: AR10935 with a non-rotating sunspot. These images are taken from url <http://www.solarmonitor.org>.

change during the disk passage while the small sunspot in the southern part exhibited rapid counterclockwise rotation about its umbral center. This sunspot started to rotate after mid day on 10 December 2006, continued to rotate until 13 December 2006 and finally produced a large X-3.4 class flare. However, sunspots in the other two active regions did not show any evidence of their rotation within their penumbral boundaries, hence they are referred to as “non-rotating” sunspots.

Our analysis utilizes high-resolution continuous Doppler data obtained by the Global Oscillation Network Group (GONG) and 96-min cadence magnetograms from the MDI onboard *Solar and Heliospheric Observatory* (SOHO). The start and end times of the various data sets used here are given in Table 1. While Dopplergrams are used to infer components of horizontal velocity using the ring-diagram method, the magnetograms provide estimates of a magnetic activity

**Table 1.** Details of active regions analyzed.

CR	Active region	Day number	Start		End		Location		CR
			Date	Time <sup>a</sup>	Date	Time <sup>a</sup>	Long	Lat	
2016	10923	1	12-Nov-06	09:01	13-Nov-06	13:00	-19.00°	-4°	5.9°
		2	13-Nov-06	09:01	14-Nov-06	13:00	-5.82°	-4°	5.9°
		3	14-Nov-06	09:01	15-Nov-06	13:00	7.36°	-4°	5.9°
		4	15-Nov-06	09:01	16-Nov-06	13:00	20.54°	-4°	5.9°
2017	10930	1	09-Dec-06	10:01	10-Dec-06	12:00	-19.00°	-4°	9.5°
		2	10-Dec-06	10:01	11-Dec-06	12:00	-5.82°	-4°	9.5°
		3	11-Dec-06	10:01	12-Dec-06	12:00	7.36°	-4°	9.5°
		4	12-Dec-06	10:01	13-Dec-06	12:00	20.54°	-4°	9.5°
2018	10935	1	05-Jan-07	17:55	06-Jan-07	21:54	-19.00°	-4°	9.5°
		2	06-Jan-07	17:55	07-Jan-07	21:54	-5.82°	-4°	9.5°
		3	07-Jan-07	17:55	08-Jan-07	21:54	7.36°	-4°	9.6°
		4	08-Jan-07	17:55	09-Jan-07	21:54	20.54°	-4°	9.6°

<sup>a</sup> All times are in UT.

index (MAI) as a measure of solar activity. To obtain the MAI, we convert magnetogram data to absolute values, average over the length of a ring day and apodise them into circular areas to match the size of the Dopplergram patches used in the ring-diagram analysis. The temporal variation of MAI in all three active regions is plotted in Figure 2. It is seen that while the average magnetic flux for ARs 10923 and 10930 has an increasing trend with time, it decreases for AR 10935, thus we categorize the former two as emerging active regions and the later as decaying. Since we do not have the resolution to discriminate between sunspots of different topology within the same active region for a meaningful analysis using ring-diagram technique, we will consider AR 10930 as a “rotating sunspot” and, ARs 10923 and 10935 as “non-rotating sunspots”.

#### 4. Analysis and Results

In this Section, we derive the subsurface horizontal velocity and its variation with time for each active region. It should be noted that areas used here are smaller in size than those used in the standard ring-diagram analysis where areas of  $16^\circ \times 16^\circ$  are generally analyzed (Haber *et al.*, 2000; Corbard *et al.*, 2003; Komm *et al.*, 2008). The analysis of smaller areas is particularly useful in the study of active regions where we can minimize the influence of relatively quiet neighboring areas (Jain *et al.*, 2010, 2011a). However, major disadvantages of this selection combined with the spatial resolution of images and the limitation

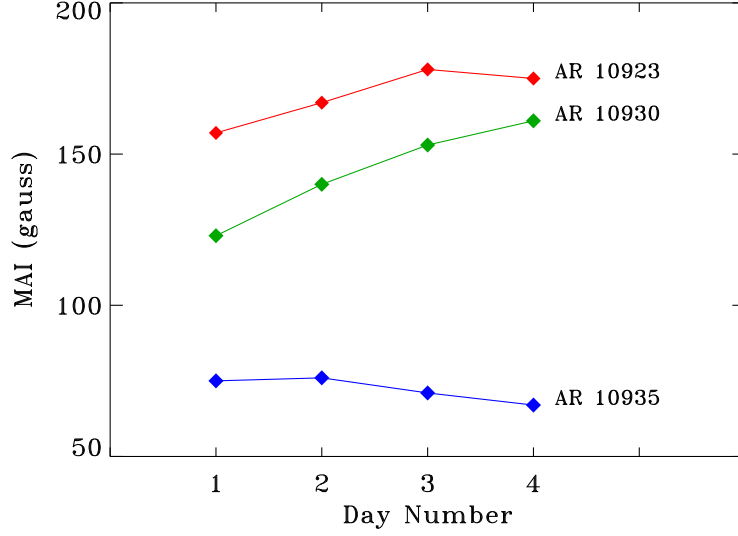


**Figure 2.** Temporal variation of magnetic activity index (MAI) in three active regions.

of the ring-diagram technique include restrictions on i) fitted modes that are available for inversion and, ii) the depth range that can be probed reliably. In this article, we discuss the relative variation in both zonal and meridional components of the horizontal velocity with time at ten target depths in the range from surface to about 12 Mm. The magnitudes are different from those reported in previous articles using ring-diagram technique (*e.g.* Komm, Howe, and Hill, 2011; and references therein) where residuals, obtained by removing large scale flows from inverted velocities, were widely studied.

In order to investigate the temporal evolution of horizontal velocity beneath active regions in various time samples, the first step is to eliminate the influence of systematic effects, if any. One potential source of error is the effect of projection that may arise due to the change in location of tracked regions from day to day during the disk passage (Komm, Howe, and Hill, 2011). Since the ring-diagram technique is sensitive to such effects, it is necessary to ensure that our inferred values are not affected by such systematics. To overcome this artifact, we calculate reference velocities in several quiet regions at the same heliographic locations as for the active regions given in Table 1 and their surrounding regions. We derive best estimates of the quiet-Sun velocities by using error-weighted averages of eight ring days with no noticeable magnetic activity on the visible disk chosen from Carrington rotations considered in this analysis.

Figure 3 shows the variation of average  $x$  (zonal) and  $y$  (meridional) components of the horizontal velocity, ( $V_x$  and  $V_y$ ), as a function of depth for quiet regions at the same four locations as active regions. As expected, in all cases, the magnitude of both  $V_x$  and  $V_y$  increases with depth. This is consistent with observations where rotation rate near the equator is found to increase with depth in the outer 5% of the Sun and also the meridional component is poleward. Negative values of  $V_y$  indicate the south-poleward direction of the meridional component

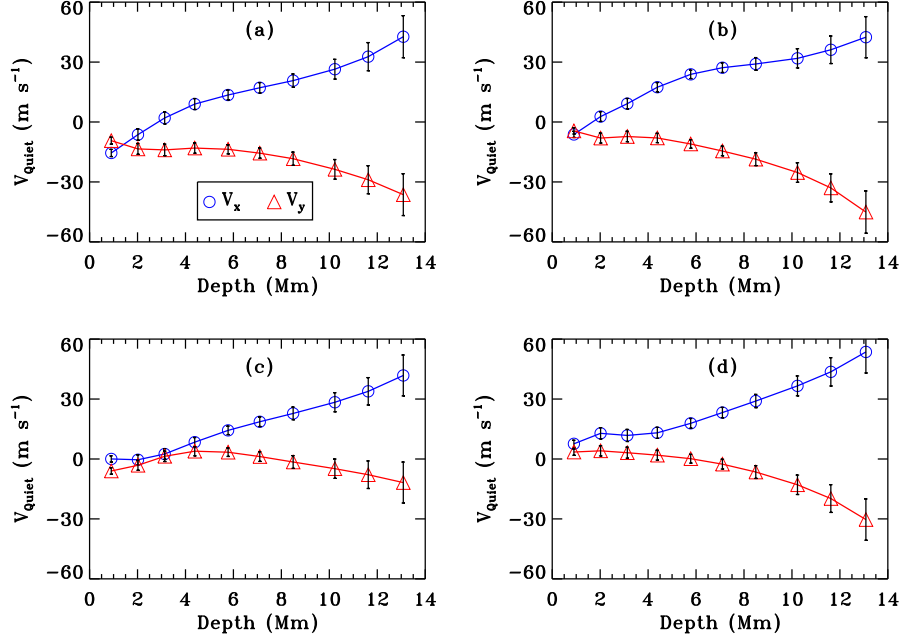


**Figure 3.** Depth variation of average  $V_x$  (blue circles) and  $V_y$  (red triangles) for quiet regions at four different locations along latitude  $4^\circ\text{S}$ . The heliocentric longitudes are: (a)  $19^\circ\text{E}$ , (b)  $5.82^\circ\text{E}$ , (c)  $7.36^\circ\text{W}$  and (d)  $20.54^\circ\text{W}$ .

of the velocity. These profiles will be used to eliminate the contribution of quiet regions from the velocity components of active regions. As mentioned above, the projection effects in both quiet and active regions are expected to be similar at same heliographic locations. Hence, we subtract average velocities of quiet regions from the calculated velocities in and around active regions. This ensures that systematic effects as well as zonal and meridional components of quiet regions are removed from the active region values which are discussed below.

#### 4.1. Rotating and Non-rotating Sunspot Regions

Figures 4 and 5 show the variation of  $V_x$  and  $V_y$  with depth for four epochs for ARs 10923 and 10930, respectively. Both components are seen to exhibit a systematic variation with depth.  $V_x$  is predominantly positive in all cases, independent of the epoch, which clearly shows that the zonal component in active regions is faster than in the quiet region. Comparing Figures 4 and 5, we find much higher  $V_x$  in the emerging region AR 10923 than the decaying AR 10935. In addition, the MAI for AR 10923 is significantly higher with rapidly increasing trend for the first few days while this variation is opposite for AR 10935. Thus, the zonal component in the strong emerging-flux region exhibits considerable variation with depth while it is comparable in the decaying-flux region to that of quiet regions. These findings support the previous analysis



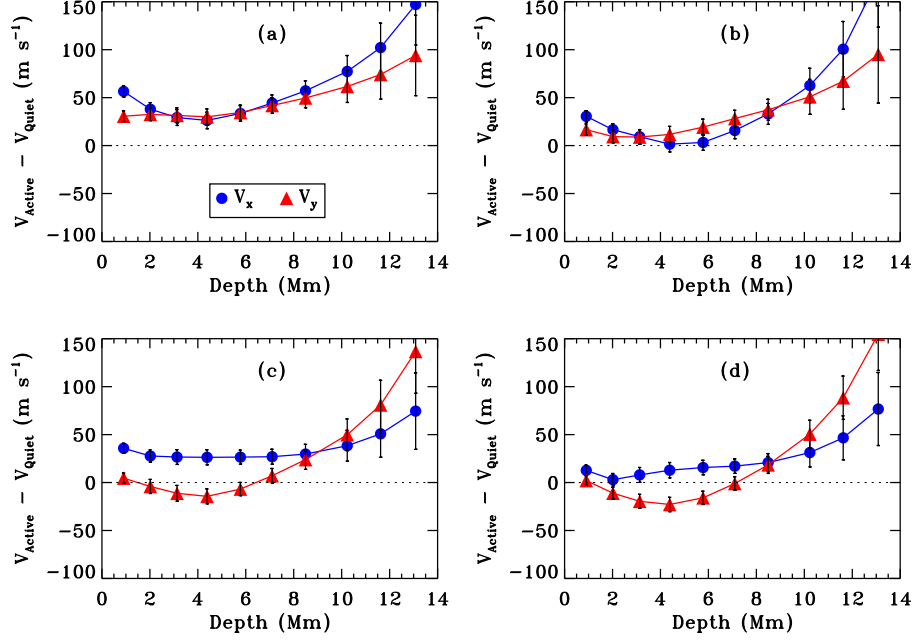


**Figure 4.** Depth variation of  $V_x$  (blue circles) and  $V_y$  (red triangles) for an emerging active region (AR 10923) consisting of non-rotating sunspots for four different epochs given in Table 1; (a) Day 1, (b) Day 2, (c) Day 3, and (d) Day 4. Values are plotted at target depths only.

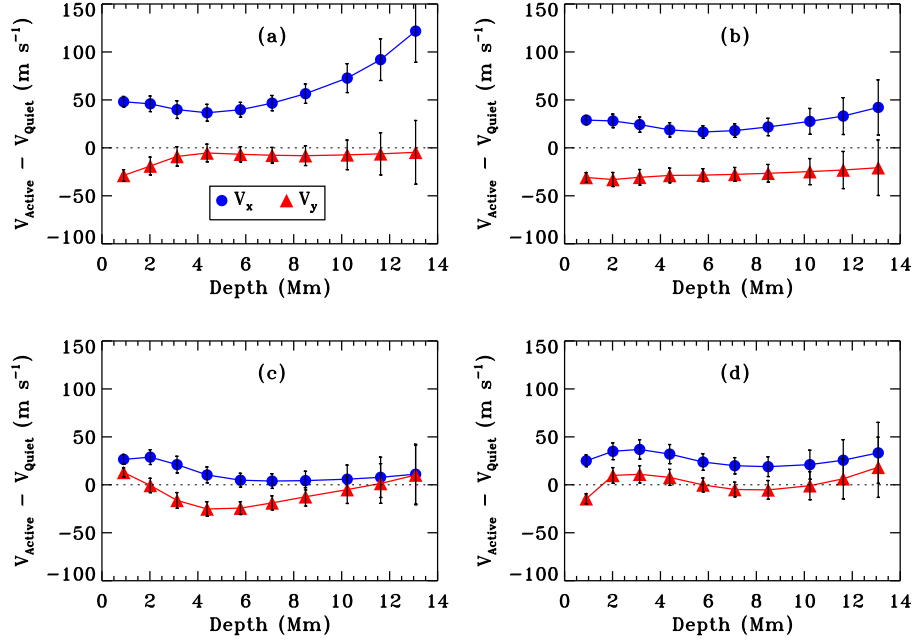


**Figure 5.** Depth variation of  $V_x$  (blue circles) and  $V_y$  (red triangles) for a decaying active region (AR 10935) consisting of non-rotating sunspots for four epochs given in Table 1; (a) Day 1, (b) Day 2, (c) Day 3, and (d) Day 4. Values are plotted at target depths only.



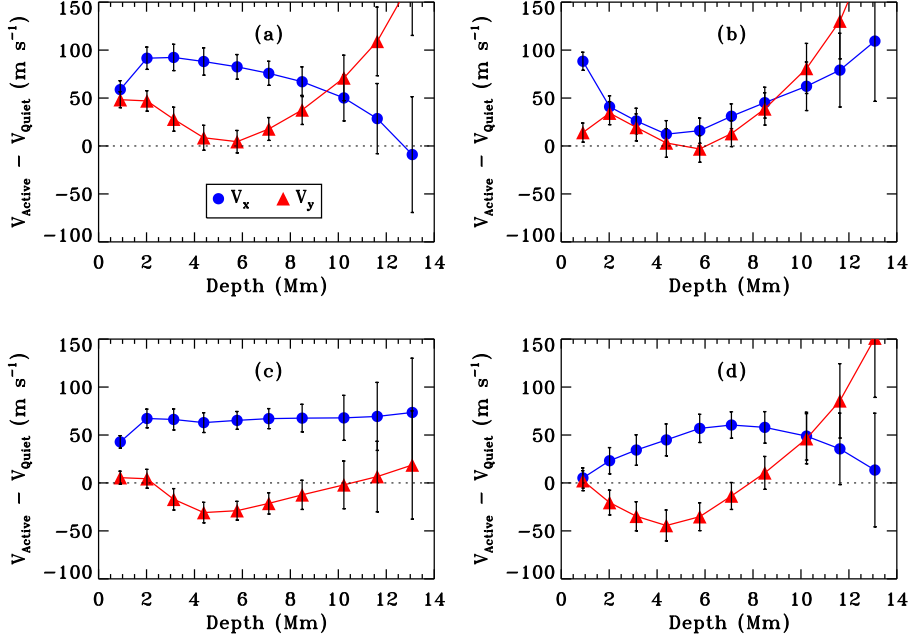


**Figure 6.** Depth variation of  $V_x$  (blue circles) and  $V_y$  (red triangles) for an active region (AR 10930) consisting of rotating and non-rotating sunspots for four epochs given in Table 1; (a) Day 1, (b) Day 2, (c) Day 3, and (d) Day 4. Values are plotted at target depths only.

(*e.g.* Komm, Howe, and Hill, 2011) where average flows for a large number of emerging and decaying active regions were studied. In contrast, the meridional component exhibits a different behavior. It increases sharply in deeper layers for the emerging-flux region while it remains mostly unchanged in the case of the decaying active region.

In Figure 6, we display similar plots for AR 10930 where one of the sunspots rotates around its umbral center. In contrast to other two active regions, the zonal component associated with this active region varies significantly with depth from one day to another. Although it remains positive for all ring days, similar to other active regions, the depth profile changes abruptly. Also, while the depth profile of the meridional component is similar for all four time samples, these exhibit significant variations in magnitude. To understand these observations, we focus on the depth range between 2 Mm and 12 Mm, where the errors are relatively small due to the set of modes contained in the analysis combined with the limitations of the model used near the surface. Below 2 Mm, we find that  $V_x$ , prior to the sunspot rotation (Figure 6(a)), decreases rapidly in deeper layers while its magnitude in Figure 6(b) first decreases up to 5 - 6 Mm and then increases. Note that Figure 6(b) includes the initial period of sunspot rotation. Further,  $V_x$  does not change significantly in Figure 6(c) and finally, it shows a trend opposite to that was seen in Figure 6(b).

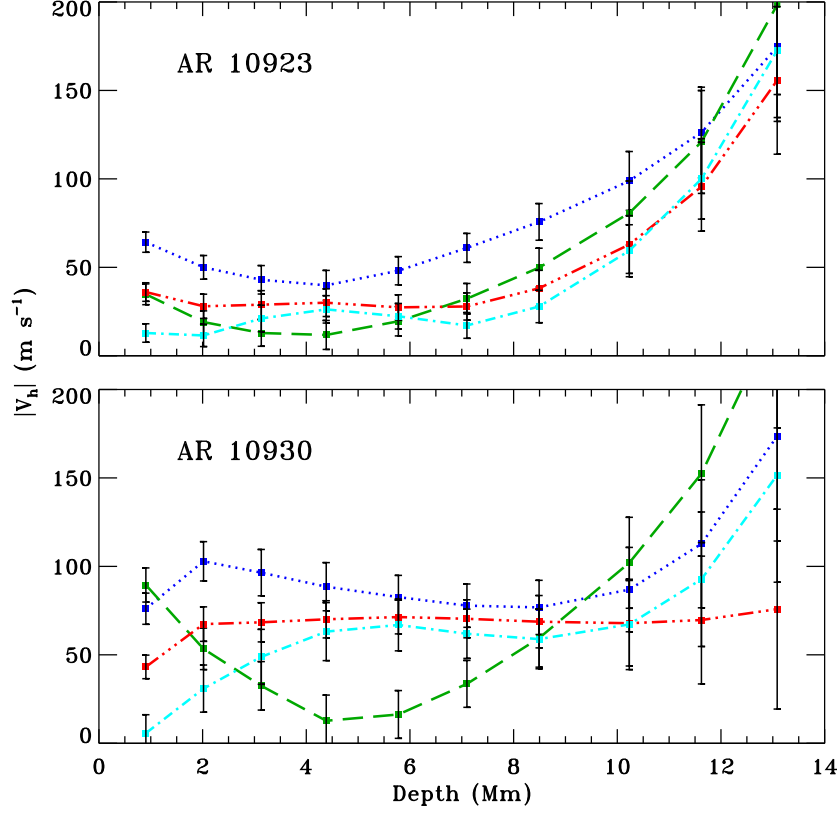


**Figure 7.** Variation of total horizontal flow as a function of depth for emerging flux regions AR 10923 (upper panel) and 10930 (lower panel) for four overlapping time intervals given in Table 1; (blue dotted) Day 1, (green dashed) Day 2, (red dashed-dot-dot-dot) Day 3, and (cyan dashed-dot) Day 4. Values are plotted at target depths only.

To interpret the physical origin of the sudden changes in the depth profiles of AR 10930 with time, we compare its inferred velocities with those of AR 10923. Although, in both cases, the magnetic flux is increasing with time, there is a significant difference in the morphology of these regions; AR 10930 has a sunspot rapidly rotating in the counter-clockwise direction while all sunspots in AR 10923 are non-rotating. Despite the temporal variation in MAI for AR 10923, its depth profile, in the absence of sunspot rotation, does not show any significant variation from one day to another while the rotation in AR 10930 is associated with changes for different time samples. This can be easily seen in Figure 7 where we plot the total horizontal velocity, defined as the square root of the sum of the squares of the velocity components. AR 10923 has smooth and similar variations with depth for all four days, while AR 10930 displays significant variation. The maximum change is seen at the beginning of sunspot rotation (Day 2) where total velocity decreases up to 4–5 Mm and then increases sharply

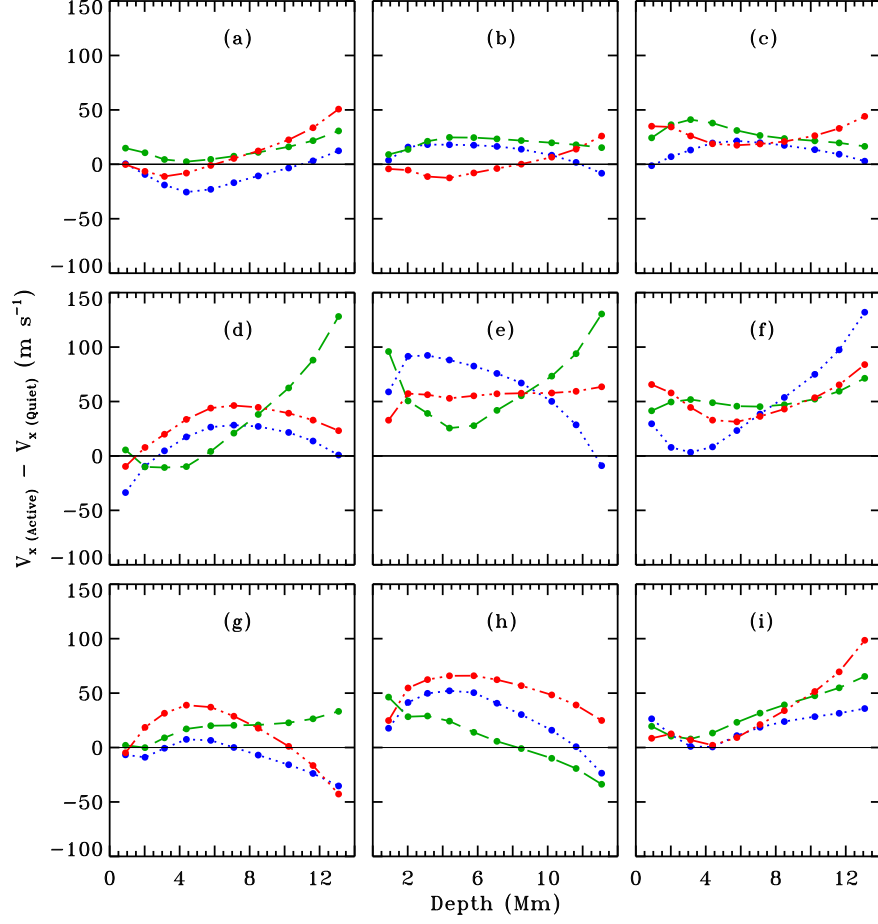


**Figure 8.** Depth variation of  $V_x$  in and around AR 10930 for three overlapping time series; blue dotted, green dashed and red dashed-dot-dot lines represent variation for Days 1, 2, and 3, respectively. Errors are of the same order as in Figure 6. The active region is located at the center of Panel (e).

in deeper layers providing an evidence for flows in two different directions. This is in agreement with Zhao and Kosovichev (2003) who report opposite flows in a rotating sunspot group (AR 9114), but this feature is absent in a non-rotating sunspot group.

#### 4.2. Surrounding Regions

It has been shown earlier that sub-surface flows in areas containing active regions are larger than their quieter surroundings (Komm *et al.*, 2005). Here we extend this analysis to quiet areas surrounding the rotating and non-rotating sunspots and analyze a mosaic of nine regions for three consecutive ring days. The central

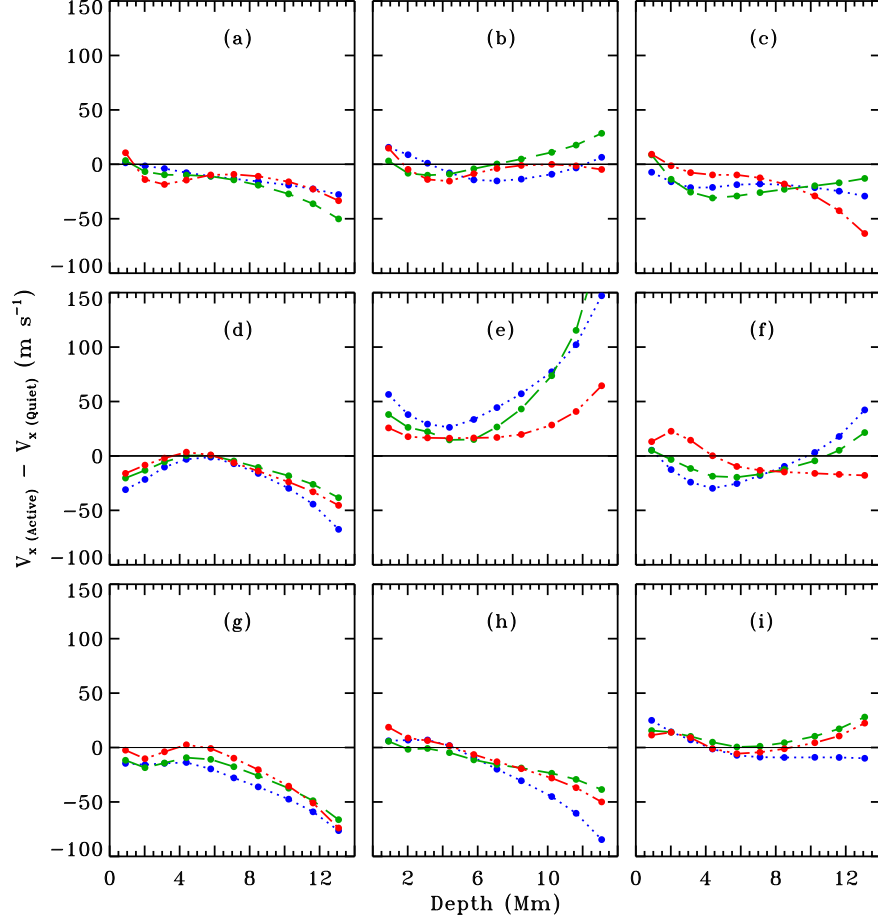


**Figure 9.** Depth variation of  $V_x$  in and around AR 10923 for three overlapping time series; blue dotted, green dashed and red dashed-dot-dot lines represent variation for Days 1, 2, and 3, respectively. Errors are of the same order as in Figure 4. The active region is located at the center of Panel (e).

region in each mosaic has the complete active region at its center (Panel (e) of Figures 8 through 11) while the neighboring eight regions, spaced by  $5^\circ$  in each direction from the central region, are relatively quiet as they include only a part of the active region. The results for the temporal variation of zonal and meridional components around ARs 10930 and 10923 are shown in Figures 8 through 11; Figures 8 and 9 focus on the variation of the zonal components, while Figures 10 and 11 provide information on the meridional components. In general, it is observed that both the zonal and meridional components of the central region (Panel (e) of these figures) have the maximum variation with depth while the neighboring quiet regions with smaller magnetic flux display smaller variation.

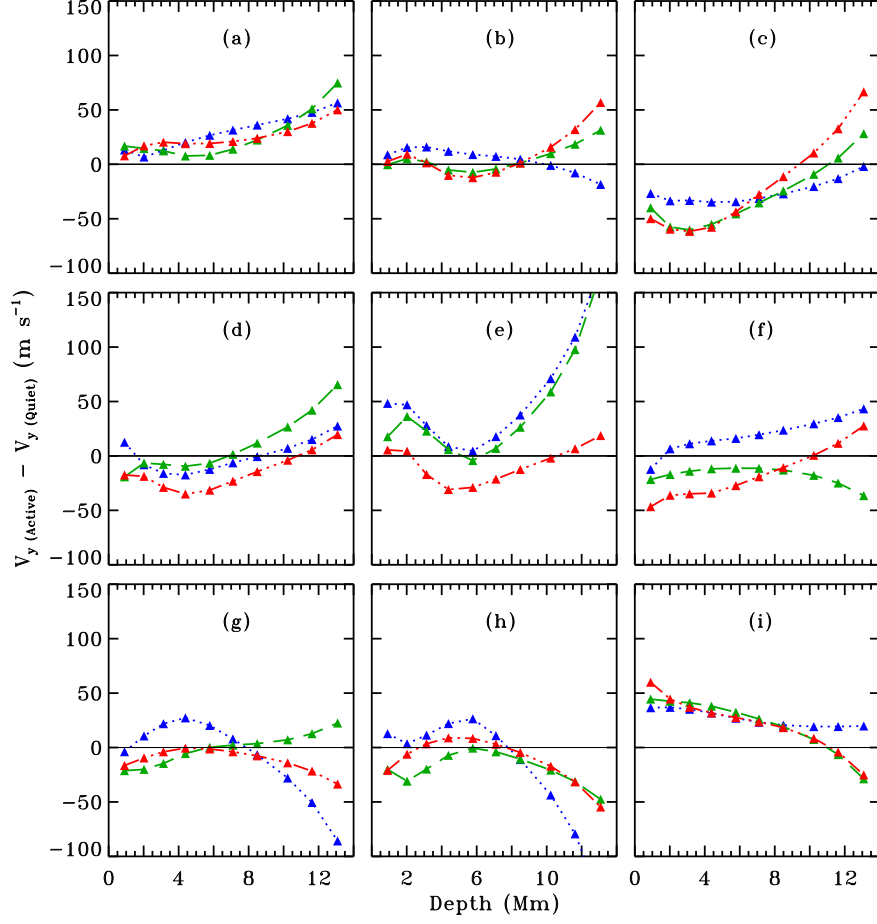


**Figure 10.** Depth variation of  $V_y$  in and around AR 10930 for three overlapping time series; blue dotted, green dashed and red dashed-dot-dot lines represent variation for Days 1, 2, and 3, respectively. Errors are of the same order as in Figure 6. The active region is located at the center of Panel (e).

On a detailed comparison of  $V_x$  of neighboring regions, we note that the depth profiles of AR 10923 for each day are comparable (within  $1\sigma$  estimates) while these are different in a few cases for AR 10930. In particular, the profiles of  $V_x$  in the regions that are adjacent to the rotating part of the AR 10930 exhibit reasonable temporal variations (shown in Panels (d), (g), and (h)) and suggest that the variation is induced by the rotation of the sunspot. Similar results are obtained for meridional components (Figures 10 and 11). This provides evidence that a rotating sunspot not only changes the flow pattern in the active region but also the flows in the surrounding areas.

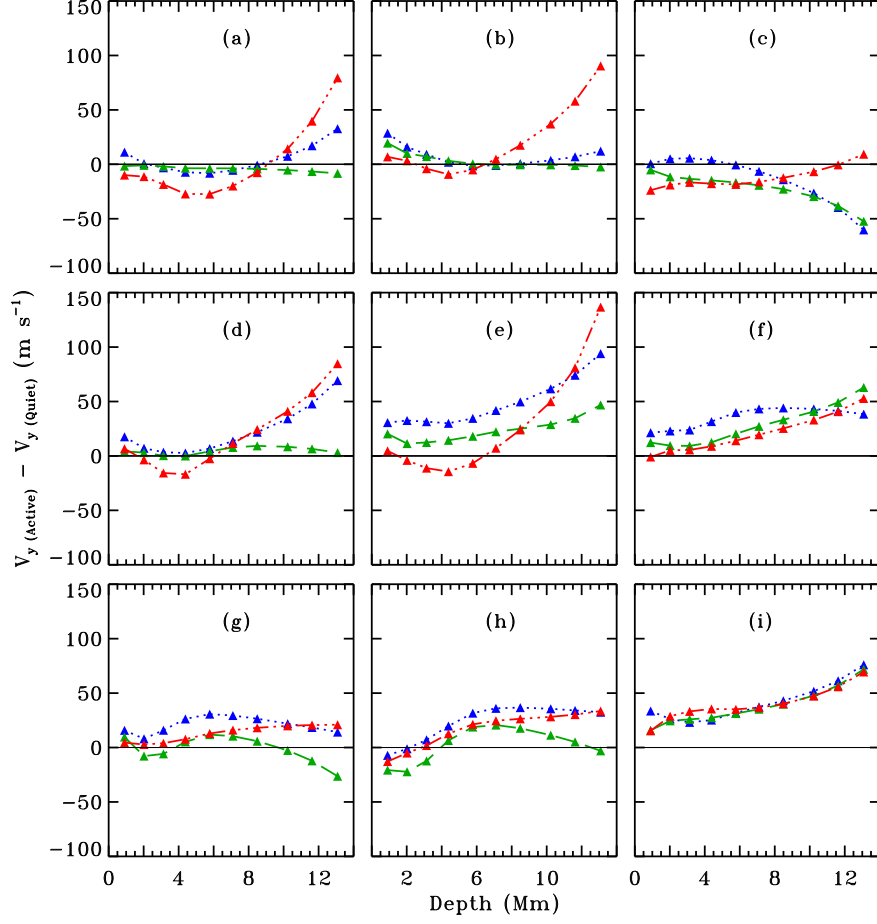


**Figure 11.** Depth variation of  $V_y$  in and around AR 10923 for three overlapping time series; blue dotted, green dashed and red dashed-dot-dot lines represent variation for Days 1, 2, and 3, respectively. Errors are of the same order as in Figure 4. The active region is located at the center of Panel (e).

## 5. Summary

We have studied the horizontal velocity in a limited number of active regions consisting of rotating and non-rotating sunspots. The analysis presented here is based on three active regions ARs 10923, 10930, 10935 from three consecutive Carrington rotations: AR 10930 contains a fast-rotating sunspot in a strong emerging active region while other two have non-rotating sunspots with emerging flux in AR 10923 and decaying flux in AR 10935. In agreement with earlier results, we note that active regions have faster zonal component as compared with the quiet regions. The variations are also found to be higher in emerging-flux regions as compared to the decaying regions. A comparison between the plasma

flow between regions with rotating and non-rotating sunspots illustrates that the flow associated with the rotating sunspot in AR 10930 varies significantly with depth during the course of the rotation while the variations in the flow in non-rotating sunspot groups, ARs 10923 and 10935, are primarily constant (within  $1\sigma$ ). We further find evidence of two opposite flows at different depth and conjecture that this opposite flow provides a twist in magnetic field lines. We illustrate that the flows in areas surrounding the active region in both cases are relatively small, but there is a significant variation in regions neighboring to the rotating sunspot.

In the present study, a sunspot group consisting of both rotating and non-rotating sunspots is considered as a rotating sunspots as a whole, thus a complete picture of the sub-surface flows beneath a rotating sunspot could not be obtained. This is mainly due to the limitations imposed by the spatial resolution on the technique. Although we have found significant differences between the temporal variations in depth profiles of rotating and non-rotating sunspots, the analysis of smaller areas will further provide a deeper insight into the dynamics of sub-surface layers below individual sunspots. We plan to carry out a detailed study using images with improved spatial resolution from the Helioseismic Magnetic Imager (HMI) onboard *Solar Dynamics Observatory* (SDO) that will allow us to analyze smaller regions within an active region. Our preliminary analysis using HMI Dopplergrams clearly shows that the ring-diagram technique can be reliably applied to regions as small as  $5^\circ$  (Jain *et al.*, 2011b) and one can obtain a comprehensive picture of the solar sub-surface layers which is crucial for space weather studies.

**Acknowledgements** This work utilizes data obtained by the Global Oscillation Network Group (GONG) project, managed by the National Solar Observatory, which is operated by AURA, Inc. under a cooperative agreement with the National Science Foundation. The data were acquired by instruments operated by the Big Bear Solar Observatory, High Altitude Observatory, Learmonth Solar Observatory, Udaipur Solar Observatory, Instituto de Astrofísica de Canarias, and Cerro Tololo Interamerican Observatory. It also utilizes data from the Solar Oscillations Investigation/Michelson Doppler Imager on the Solar and Heliospheric Observatory. SOHO is a mission of international cooperation between ESA and NASA. This work was partially supported by NASA grant NNG08EI54I and NSF Award 1062054 to the National Solar Observatory.

## References

- Antia, H.M., Basu, S.: 2007, Local helioseismology using ring diagram analysis. *Astron. Nach.* **328**, 257.
- Baldner, C.S., Bogart, R.S., Basu, S.: 2011, Evidence for solar frequency dependence on sunspot type. *Astrophys. J. Lett.* **733**, L5.
- Basu, S., Antia, H.M., Bogart, R.S.: 2004, Ring-diagram analysis of the structure of solar active regions. *Astrophys. J.* **610**, 1157.
- Bogart, R.S., Basu, S., Rabello-Soares, M.C., Antia, H.M.: 2008, Probing the subsurface structures of active regions with ring-diagram analysis. *Solar Phys.* **251**, 439.
- Brown, D.S., Nightingale, R.W., Alexander, D., Schrijver, C.J., Metcalf, T.R., Shine, R.A., Title, A.M., Wolfson, C.J.: 2003, Observations of rotating sunspots from TRACE. *Solar Phys.* **216**, 79.



- Corbard, T., Toner, C., Hill, F., Hanna, K.D., Haber, D.A., Hindman, B.W., Bogart, R.S.: 2003, Ring-diagram analysis with GONG++. In: Sawaya-Lacoste, H. (ed.) *GONG+ 2002. Local and Global Helioseismology: the Present and Future, ESA Special Publication* **517**, 255.
- Evershed, J.: 1909, Radial movement in sun-spots. *Mon. Not. Roy. Astron. Soc.* **69**, 454.
- Gizon, L., Birch, A.C., Spruit, H.C.: 2010, Local helioseismology: three-dimensional imaging of the solar interior. *Ann. Rev. Astron. Astrophys.* **48**, 289.
- González Hernández, I., Komm, R., Hill, F., Howe, R., Corbard, T., Haber, D.A.: 2006, Meridional circulation variability from large-aperture ring-diagram analysis of Global Oscillation Network Group and Michelson Doppler Imager data. *Astrophys. J.* **638**, 576.
- Haber, D.A., Hindman, B.W., Toomre, J., Bogart, R.S., Thompson, M.J., Hill, F.: 2000, Solar shear flows deduced from helioseismic dense-pack samplings of ring diagrams. *Solar Phys.* **192**, 335.
- Haber, D.A., Hindman, B.W., Toomre, J., Bogart, R.S., Larsen, R.M., Hill, F.: 2002, Evolving submerged meridional circulation cells within the upper convection zone revealed by ring-diagram analysis. *Astrophys. J.* **570**, 855.
- Hathaway, D.H., Wilson, R.M.: 1990, Solar rotation and the sunspot cycle. *Astrophys. J.* **357**, 271.
- Hill, F.: 1988, Rings and trumpets - three-dimensional power spectra of solar oscillations. *Astrophys. J.* **333**, 996.
- Hindman, B.W., Gizon, L., Duvall, T.L. Jr., Haber, D.A., Toomre, J.: 2004, Comparison of solar subsurface flows assessed by ring and time-distance analyses. *Astrophys. J.* **613**, 1253.
- Jain, K., Hill, F., Tripathy, S.C., González-Hernández, I., Armstrong, J.D., Jefferies, S.M., Rhodes, E.J. Jr., Rose, P.: 2008, Multi-spectral analysis of acoustic mode characteristics in active regions. In: Howe, R., Komm, R.W., Balasubramaniam, K.S., Petrie, G.J.D. (eds.) *Subsurface and Atmospheric Influences on Solar Activity, Astron. Soc. Pac. Conf. Ser.* **383**, 389.
- Jain, K., Hernández, I.G., Komm, R., Hill, F.: 2010, Subsurface flows beneath a rotating sunspot. *Astron. Nach.* **331**, P13.
- Jain, K., Komm, R., Hernández, I.G., Tripathy, S.C., Hill, F.: 2011a, Subsurface flows associated with rotating sunspots. In: Choudhary, D.P., Strassmeier, K.G. (eds.) *Physics of Sun and Star Spots, IAU Symp.* **273**, 356.
- Jain, K., Tripathy, S.C., González Hernández, I., Kholikov, S., Hill, F., Komm, R., Bogart, R., Haber, D.: 2011b, Testing the GONG ring-diagram pipeline with HMI Dopplergrams. *J. Phys: Conf. Ser.* **271**(1), 012017.
- Javaraiah, J., Bertello, L., Ulrich, R.K.: 2005, An interpretation of the differences in the solar differential rotation during even and odd sunspot cycles. *Astrophys. J.* **626**, 579.
- Knoska, S.: 1975, Rotational motions of sunspots. *Bull. Astron. Inst. Czechosl.* **26**, 151.
- Komm, R., Howe, R., Hill, F.: 2011, Subsurface velocity of emerging and decaying active regions. *Solar Phys.* **268**, 407.
- Komm, R., Corbard, T., Durney, B.R., González Hernández, I., Hill, F., Howe, R., Toner, C.: 2004, Solar subsurface fluid dynamics descriptors derived from Global Oscillation Network Group and Michelson Doppler Imager data. *Astrophys. J.* **605**, 554.
- Komm, R., Howe, R., Hill, F., González-Hernández, I., Toner, C., Corbard, T.: 2005, Ring analysis of solar subsurface flows and their relation to surface magnetic activity. *Astrophys. J.* **631**, 636.
- Komm, R., Morita, S., Howe, R., Hill, F.: 2008, Emerging active regions studied with ring-diagram analysis. *Astrophys. J.* **672**, 1254.
- Komm, R., Howe, R., Hill, F., González Hernández, I.: 2009, Subsurface zonal flows. *Solar Phys.* **254**, 1.
- López Fuentes, M.C., Démoulin, P., Mandrini, C.H., Pevtsov, A.A., van Driel-Gesztelyi, L.: 2003, Magnetic twist and writhe of active regions. on the origin of deformed flux tubes. *Astron. Astrophys.* **397**, 305.
- Min, S., Chae, J.: 2009, The rotating sunspot in AR 10930. *Solar Phys.* **258**, 203.
- Rajaguru, S.P., Basu, S., Antia, H.M.: 2001, Ring diagram analysis of the characteristics of solar oscillation modes in active regions. *Astrophys. J.* **563**, 410.
- Snodgrass, H.B.: 1984, Separation of large-scale photospheric Doppler patterns. *Solar Phys.* **94**, 13.
- Stenflo, J.O.: 1969, A mechanism for the build-up of flare energy. *Solar Phys.* **8**, 115.

- Tripathy, S.C., Wet, S., Jain, K., Clark, R., Hill, F.: 2008, Helioseismic ring analysis of CME source regions. *J. Astrophys. Astron.* **29**, 207.
- Zhao, J., Kosovichev, A.G.: 2003, Helioseismic observation of the structure and dynamics of a rotating sunspot beneath the solar surface. *Astrophys. J.* **591**, 446.

